Supplementary information

986

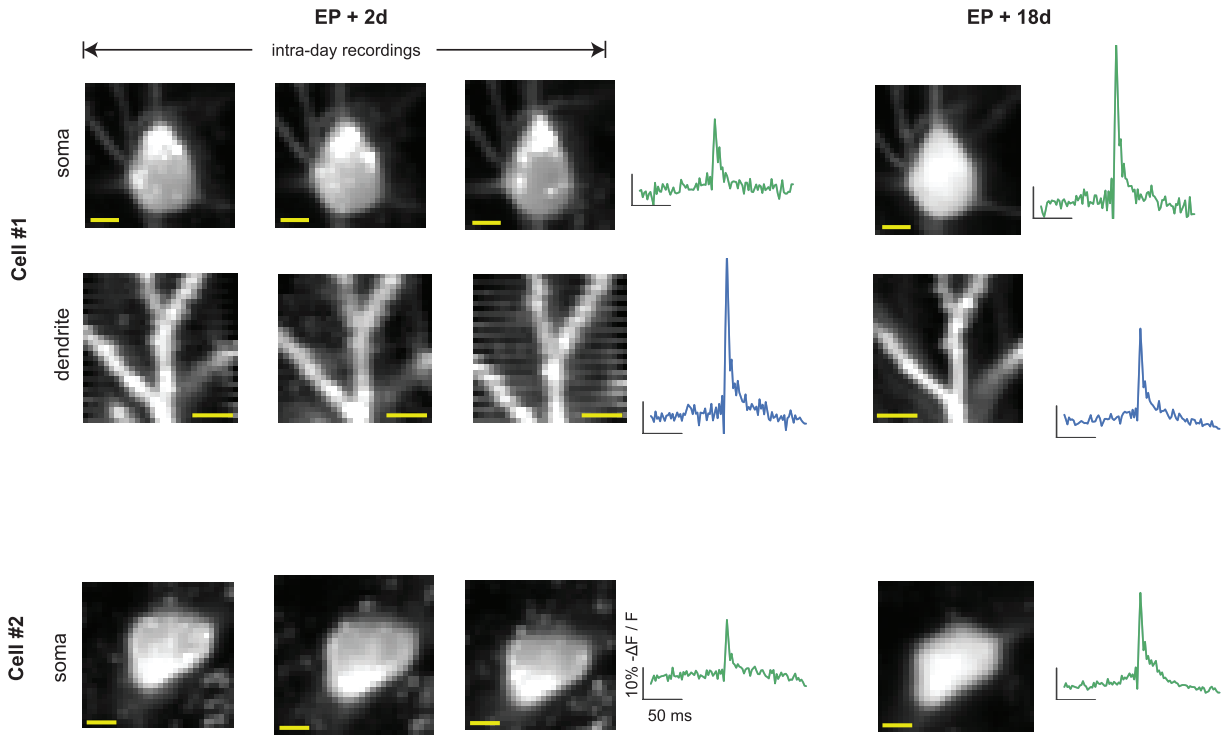

Figure S1. Cell health over time. Two example cells shown. We return to the same cell and same dendrites 2 days post-EP and 18 days post-EP and in recordings taken at multiple timepoints find the cell membrane intact with absence of noticeable apoptotic blebbing (scale bars 5μm). The mean detected DE at each ROI over all sessions is shown in the early and late recordings: waveform morphology remains stable although amplitude may change due to changes in sensor expression.

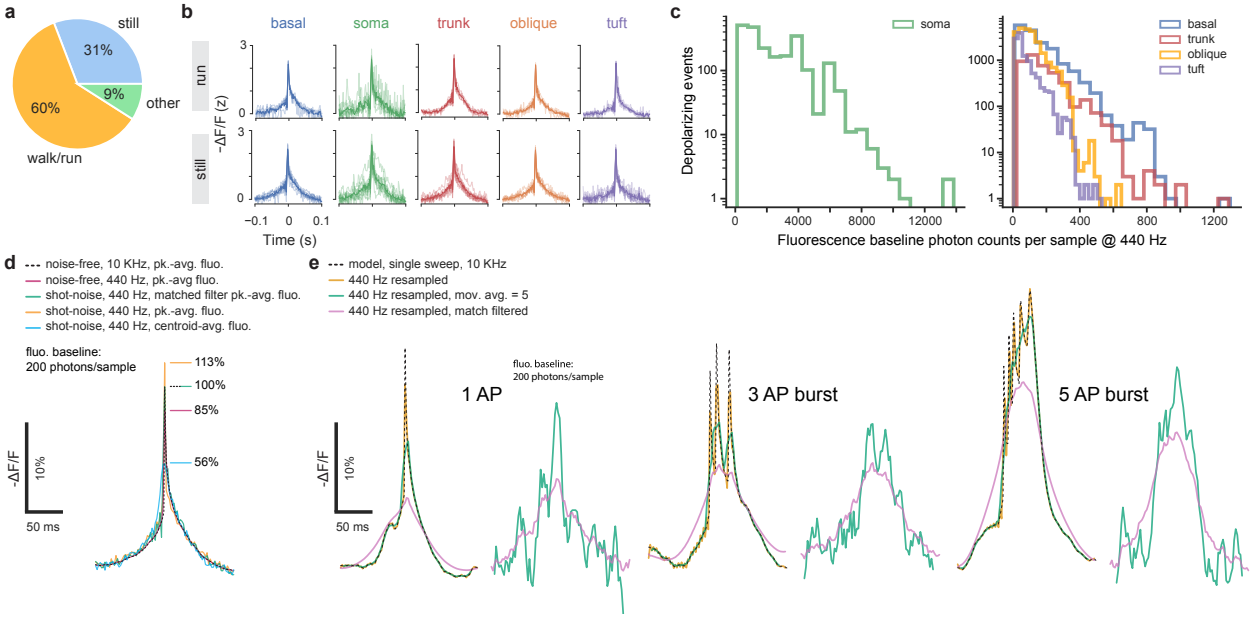

Figure S2. Extended data associated with Fig 1. a. Percent of recording time classified as locomotion, stillness, and other (transition between stillness and locomotion). **b.** Average DE waveforms (z-score) during running and stillness per dendritic region for DEs at a fluorescence baseline SNR >10. **c.** Photon counts for fluorescence baseline at time of depolarizing events (DEs) in soma (left) and dendritic domains (right) at a sampling rate of 440 Hz. **d.** Effect of downsampling to 440 Hz and choosing different methods of aligning ASAP3 Markov-model fluorescence response peaks to multiple in vivo somatically-recorded single action potentials from a mouse dorsal CA1-area hippocampal pyramidal neuron under Poisson shot-noise (200 cts/sample). Downsampling alone to 440 Hz (purple) reduced the noise-free peak-averaged response to 85% of its original value sampled at 10 KHz (black dashed). Aligning shot-noise limited waveforms by the fluorescence peaks artificially biases the peak of the average waveform (orange) to 133% of its downsampled value, while aligning waveforms using the matched-filtered signal peaks (green), the bias reduced to 118% of its downsampled value. Aligning by the centroid (cyan) of shot-noise limited waveforms severely reduced the measured peak to 66% of its downsampled value. **e.** Effect of applying a 5-point moving average filter or a matched filter to a shot-noise limited (200 cts/sample) 440 Hz recorded ASAP3 Markov-model fluorescence response to one, three and five action-potential burst waveforms. For the matched filter template, the fluorescence response to a single somatically-recorded action potential was used. Note that from the matched-filter signal it is not possible to distinguish the number or timing of action-potentials in a burst.

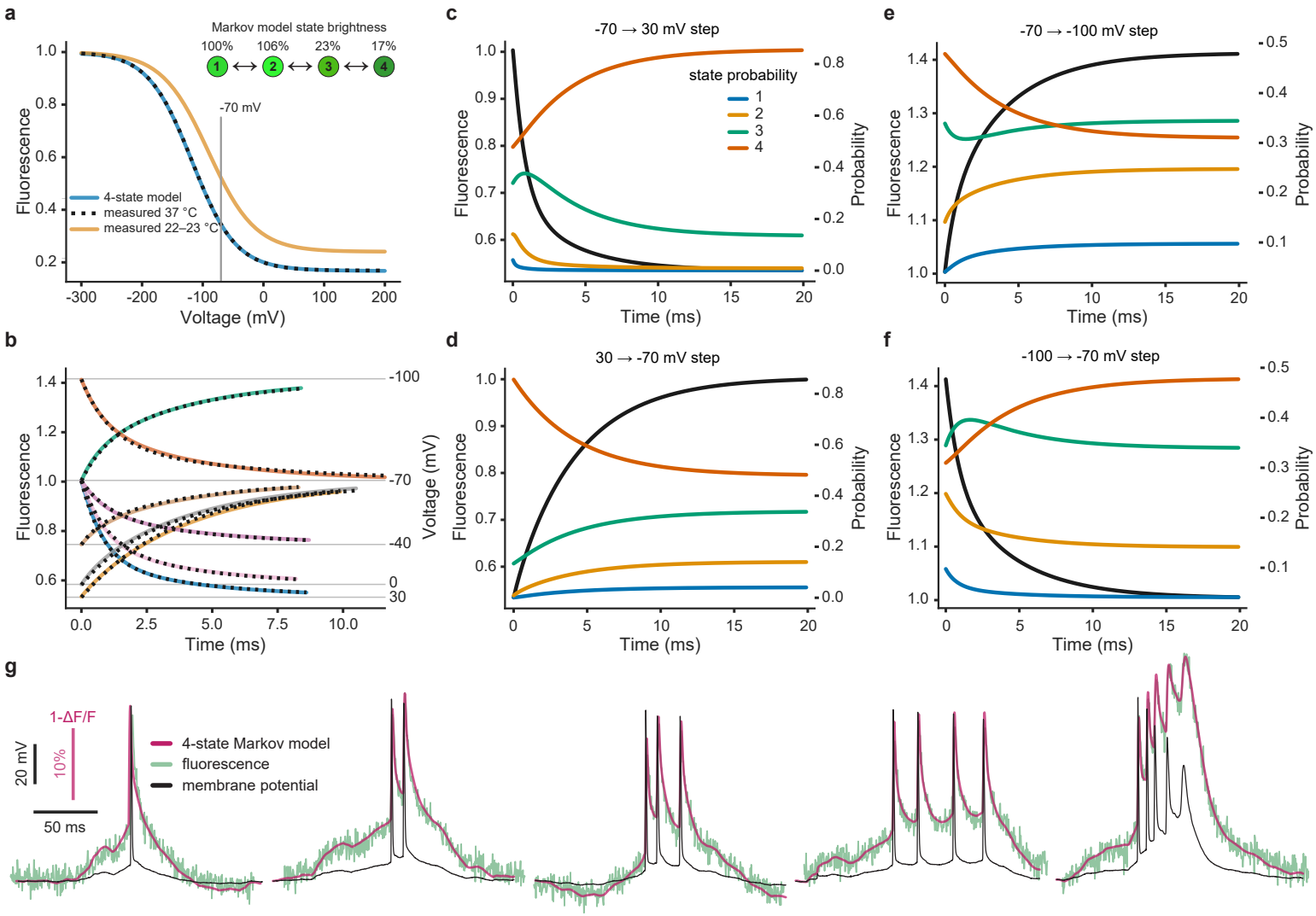

Figure S3. ASAP3 Markov model. a. Comparison of measured steady state fluorescence response at 22–23 °C (orange) and 37 °C (black dashed) and Markov model response (light blue) in voltage-clamped HEK293 cells. Note that steady state responses are temperature sensitive. Inset top: 4-state Markov chain with relative state brightness. **b.** Comparison of measured fluorescence response (black dashed) to step changes in holding potential in HEK293 cells at 37 °C and 4-state Markov model response (continuous curves). **c.–f.** Dynamic distribution of Markov model state probabilities as a function of voltage step in HEK293 cells at 37 °C. **g.** Markov model response (purple) to in-vivo measured action-potential burst waveforms (black) from a mouse dorsal hippocampal CA1-area pyramidal cell and measured fluorescence response (green) in a voltage-clamped HEK293 cell at 37 °C.

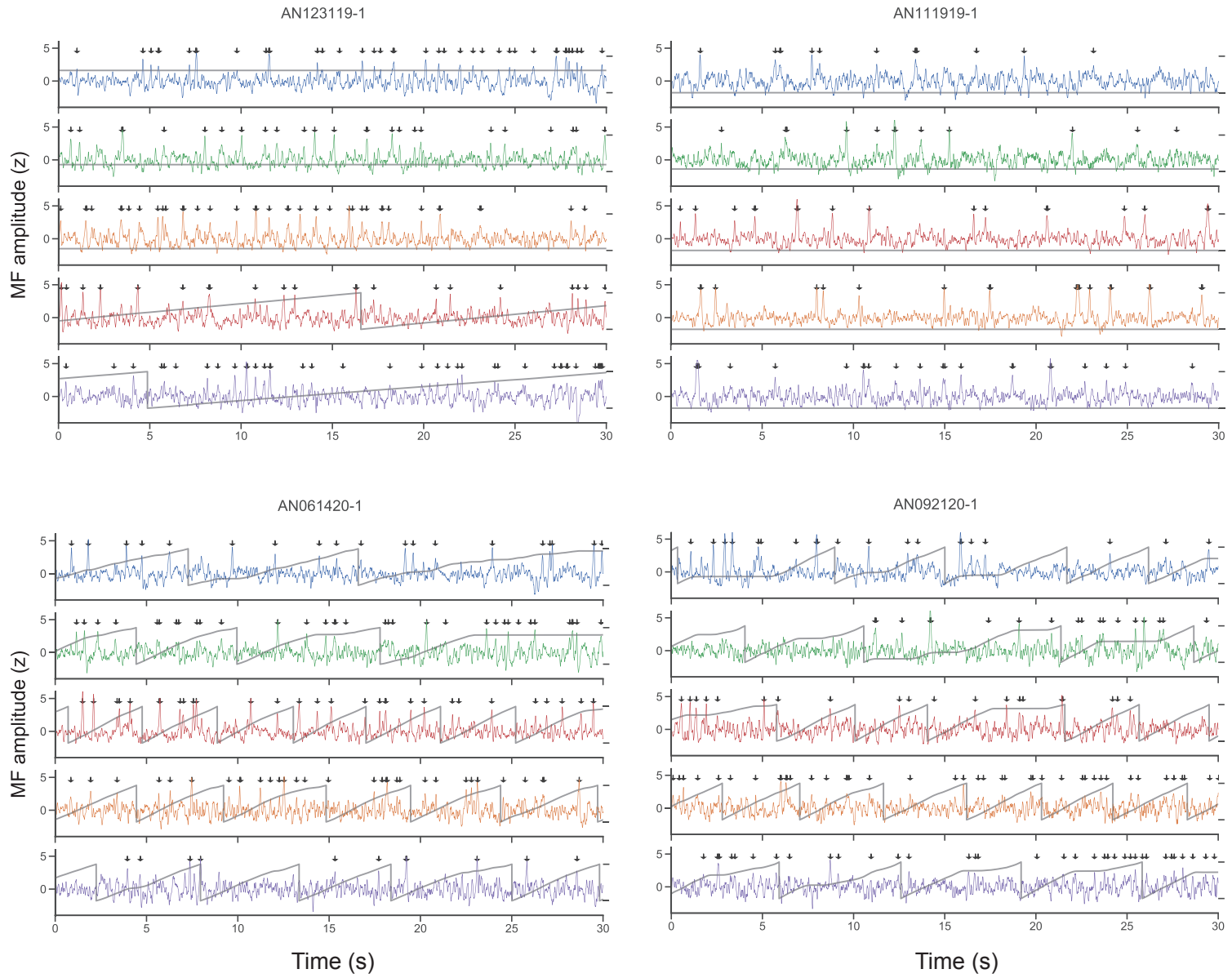

Figure S4. Further examples of raw signals from four distinct cells and compartments. As in Fig 1, signals, sampled at 440 Hz, were stabilized against movement artifacts, match-filtered (MF) and thresholded for depolarizing event (DE) detection (arrows) at a false positive rate of at most 0.01 Hz, plotted as $-\Delta F/F$ to reflect the conventional direction of change in the membrane potential. Grey traces: animal position during the recording.

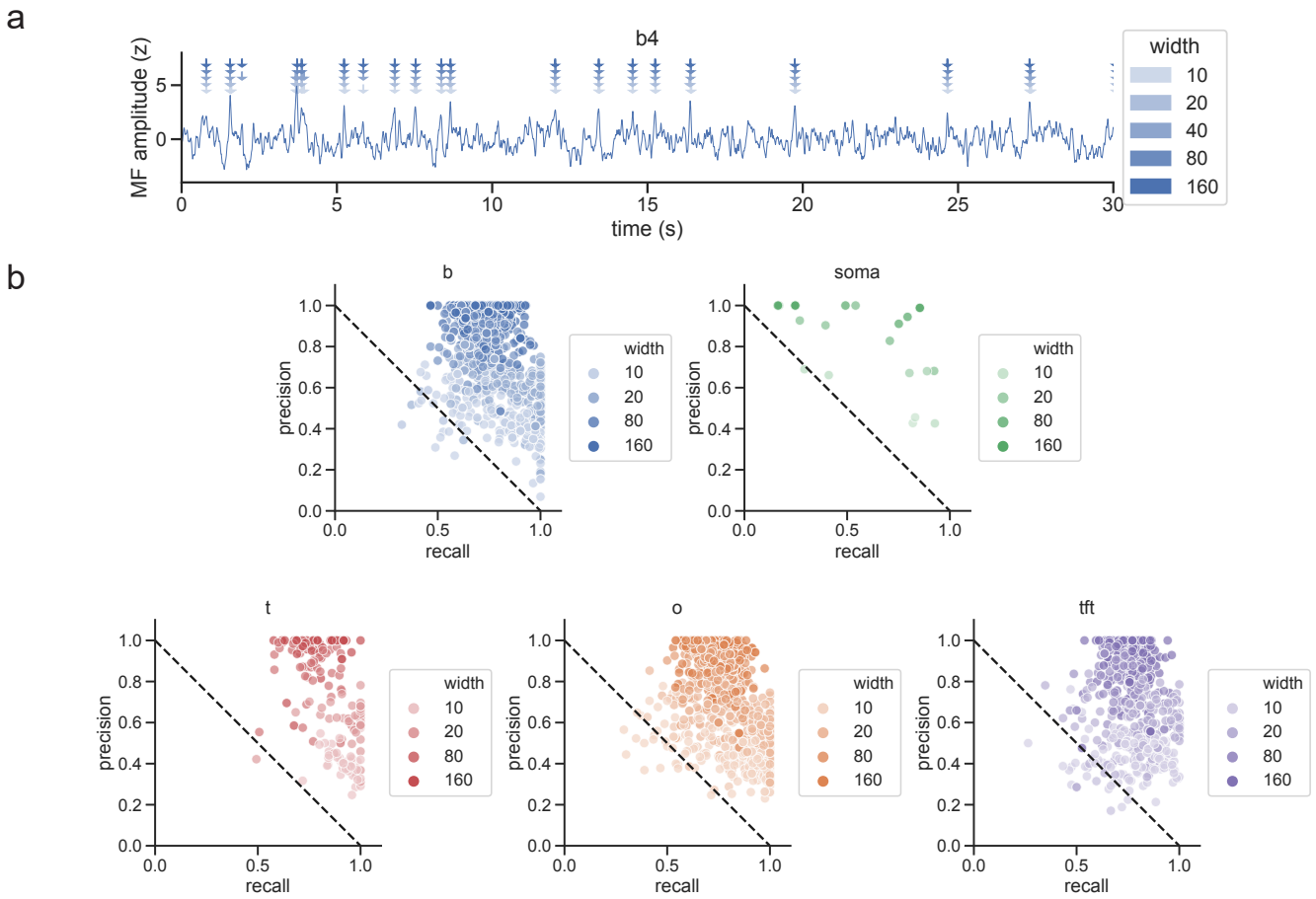

Figure S5. Detected events are robust to choice of event detection window. a. Example trace from a basal dendrite with events detected using different windows (arrows; 10 ms, 20 ms, 40 ms (default), 80 ms, 160 ms). While some variability is seen, there is agreement across all window sizes on the vast majority of events, particularly high-amplitude events. **b.** Precision-recall scatterplot by region for different choices of window size, calculated relative to the default window size (40 ms). Each point represents all events from a single dendrite. Precision is defined as # events on which the default and test window agree / total # events detected using the test window size. Recall is defined as # events on which the default and test window agree / total # events detected using the default window size. In all regions, points are concentrated in the top right in each plot indicating good agreement in detected events between different window sizes.

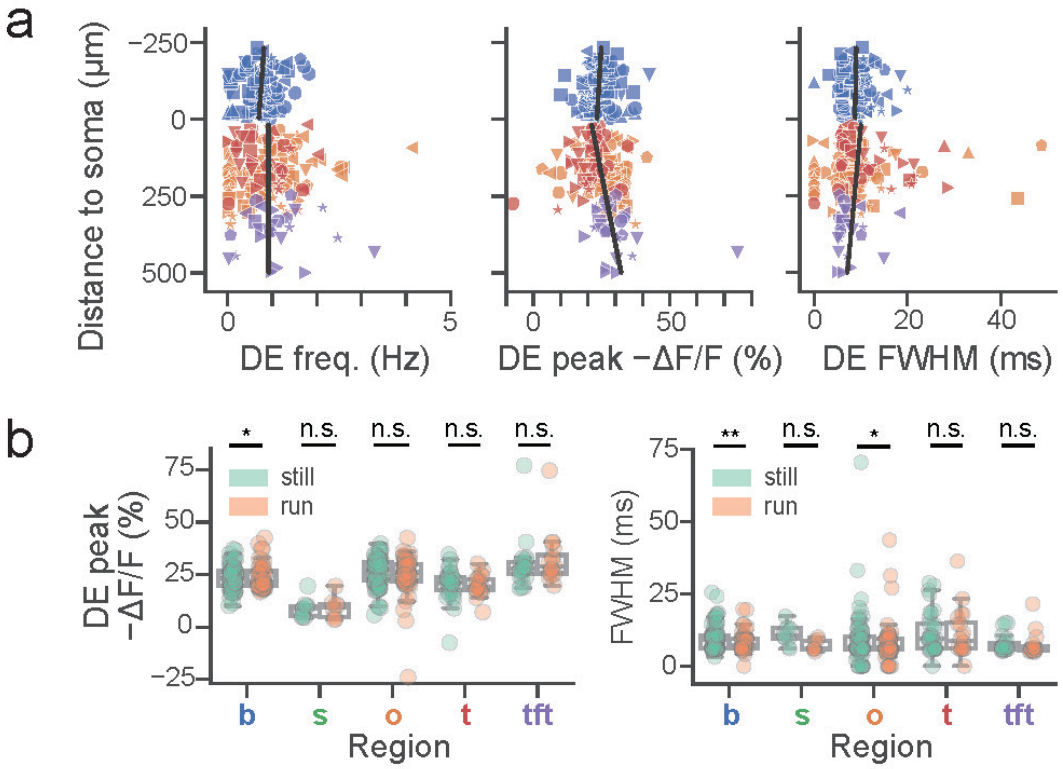

Figure S6. Basic characterization of DE parameters by domain and distance to soma. a. DE frequency (basal: slope=5×10^{-4} Hz/μm, $p = 0.43$, $r = 0.08$; apical: slope=5×10^{-6} Hz/μm, $p = 0.99$, $r = 7 \times 10^{-4}$), amplitude (basal: slope=7×10^{-3} $\%\Delta F/F/\mu$m, $p = 0.43, r = 0.08$; apical: slope=0.02 $\%\Delta F/F/\mu$m, $p = 2 \times 10^{-4}, r = 0.29$) and FWHM (basal: slope=1×10^{-3} ms/μm, $p = 0.79, r = 0.03$; apical: slope=-6×10^{-3} ms/μm, $p = 0.25, r = -0.09$) dependence on path-distance from soma across dendritic domains (same color coding) for fluorescence baseline SNR >10 ($N = 10$ cells). **b.** Left: DE amplitude is not significantly modulated between locomotion and stillness for soma ($p = 0.55$), trunk ($p = 0.06$, $N = 1 - 12$ ROIs per cell), oblique ($p = 0.43$, $N = 6 - 40$ ROIs per cell), and tuft ($p = 0.71$, $N = 1 - 11$ ROIs per cell) regions for fluorescence baseline SNR >10, $N = 10$ cells. A small but statistically significant locomotion-associated increase in amplitude was observed in the basal domain ($p = 0.01$; $N = 5 - 30$ ROIs per cell, all Wilcoxon paired test). Two-way ANOVA for amplitude: $p = 6 \times 10^{-25}$, main effect of region; $p = 0.92$, main effect of locomotion; $F(4, 401) = 0.63, p = 0.64$ region×locomotion interaction. Right: DE full-width at half-maximum (FWHM) is slightly shortened during locomotion in the basal ($p = 1.5 \times 10^{-3}$) and oblique ($p = 1.2 \times 10^{-2}$) domains. FWHM is not significantly modulated in the other domains (soma: $p = 0.11$, trunk: $p = 0.33$, tuft: $p = 0.24$; all Wilcoxon paired test). Two-way ANOVA for FWHM: $p = 0.01$, main effect of region; $p = 0.23$, main effect of locomotion; $F(4, 401) = 0.39, p = 0.82$ region×locomotion interaction.

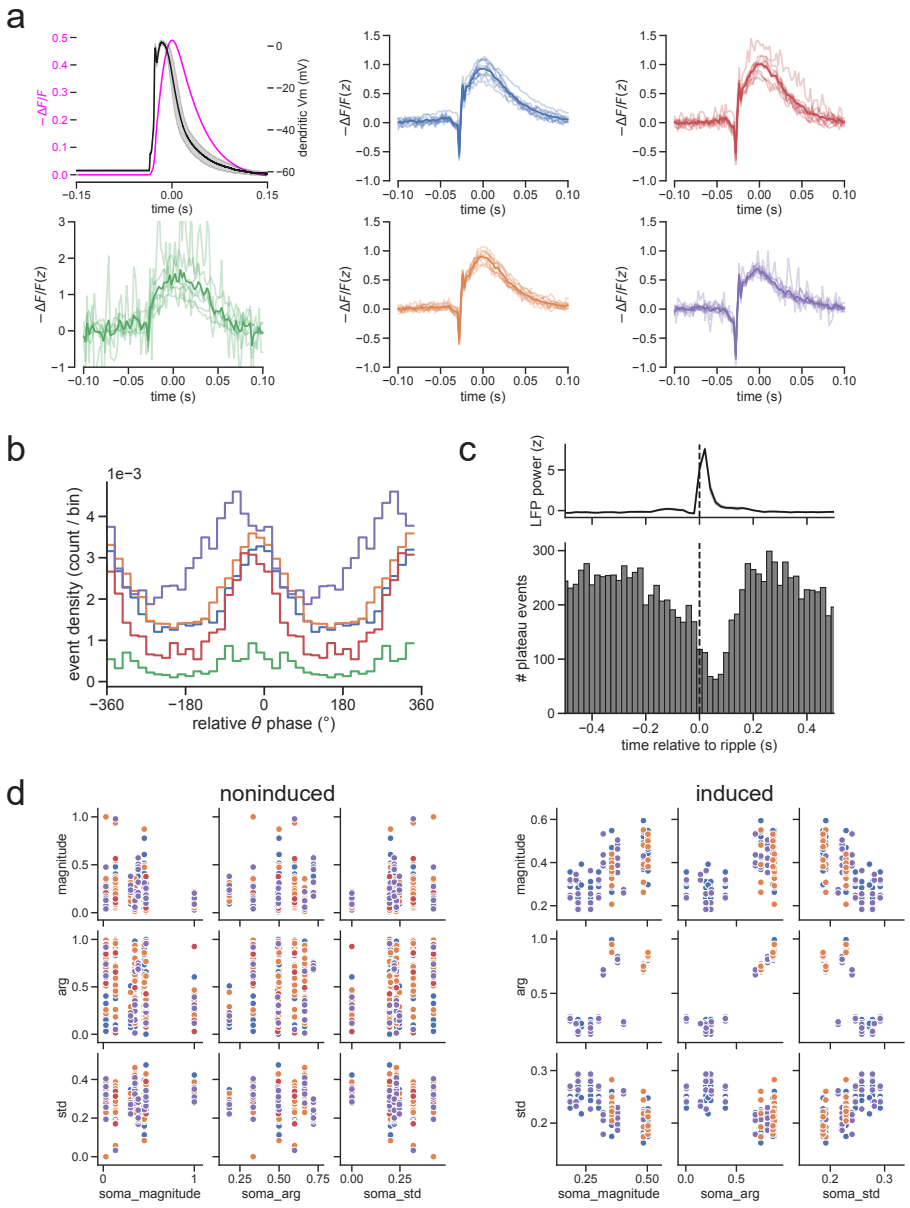

Figure S7. Basic properties of "slow" dendritic events calibrated to patch data. Slow events exhibit a qualitatively different waveform from fast (AP-like) events, with similarities and differences in other properties. **a.** Matched-filter based slow event detection from N=9 cells. Top left: Electrophysiologically recorded slow dendritic event waveform from[44] (black line; stimulation artifact removed), and model-predicted fluorescence waveform (magenta line). Colored panels: Mean slow event waveform detected in each region. Light traces: mean event from 1 cell and region. Dark trace: mean event across cells. **b.** Histogram of slow event phases by region. We note that, unlike fast events which exhibit marked phase advancement across regions (Fig 2), the distribution of slow events appears to be concentrated around 0°in all regions but the tuft. **c.** Peri-ripple slow event histogram. Dashed line: peak of LFP ripple power as in Fig 4b. Similar to fast DEs (Fig 4), slow events are suppressed around SWRs with the onset of suppression preceding the rise in ripple power, the nadir coming slightly after the ripple power peak, and a rapid return to baseline. **d.** Soma vs dendrite tuning vector relationships pre- and post place field induction. Magnitude refers to the strength of event tuning. "Arg" refers to the tuning center of mass around the circle (normalized such that 1 refers to 2π). "Std" refers to standard deviation. In the pre/non-induced dataset, there is no relationship between somatic and dendritic parameters, while after induction, consistent with our DE findings, dendrites' tuning centers shift towards their somatic tuning center; strength of somatic tuning correlates to strength of dendritic tuning and inversely to variability in dendritic tuning. Each point: 1 dendrite.

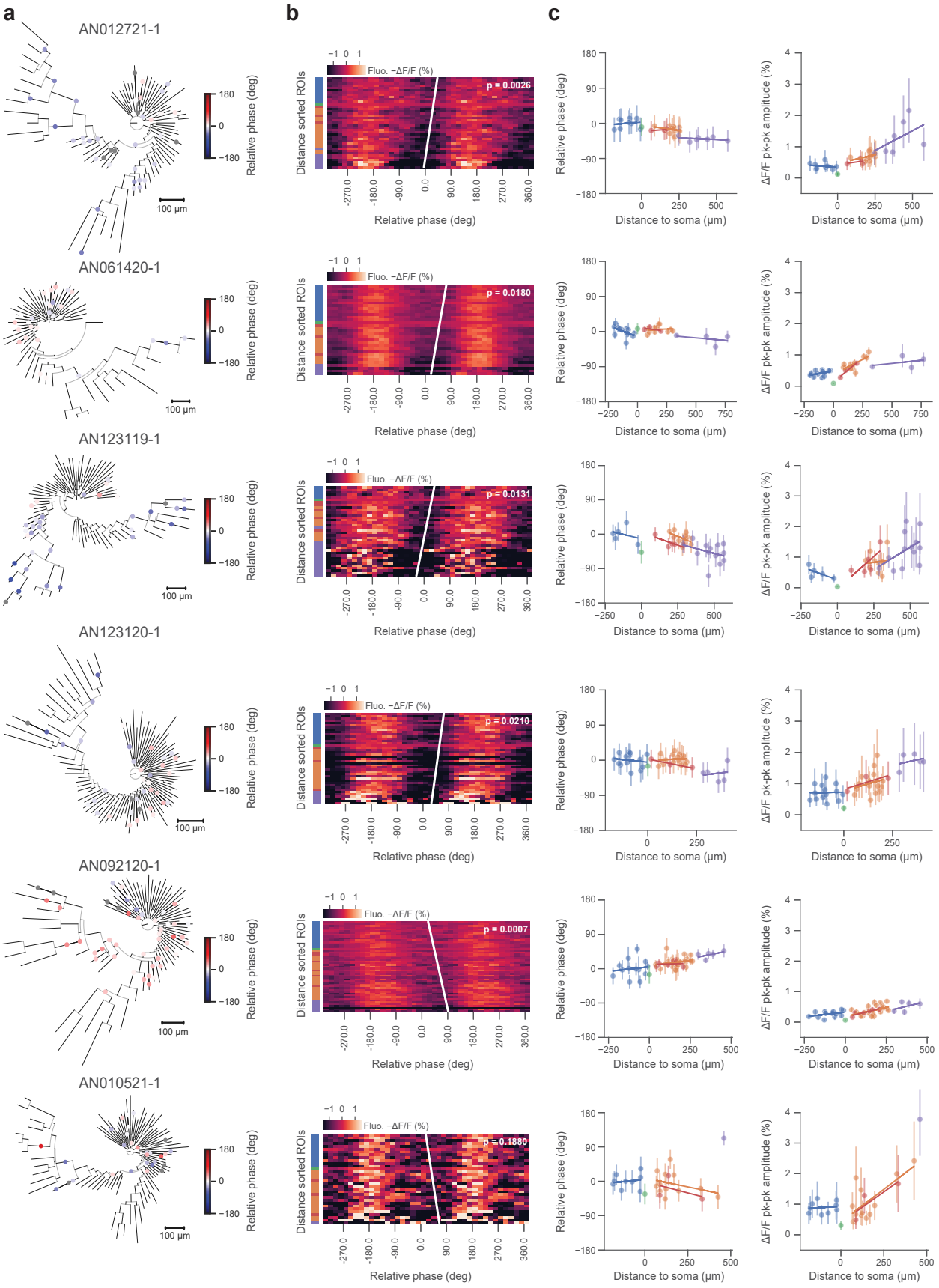

Figure S8. Extended data associated with Fig 2. Additional example cells. (caption next page)

Figure S8. Extended data associated with Fig 2. Additional example cells. a. Morphological reconstructions with theta-oscillation modulated fluorescence ROIs colored by relative phase to somatic compartment. Nonsignificantly phase modulated ROIs in grey. **b.** Membrane potential oscillation gradients for cells shown in **a.**, with rank regression line and p value shown. **c.** Per-region phase relative to somatic compartment, amplitude estimates and associated trendline fits for cells shown in **a.**.

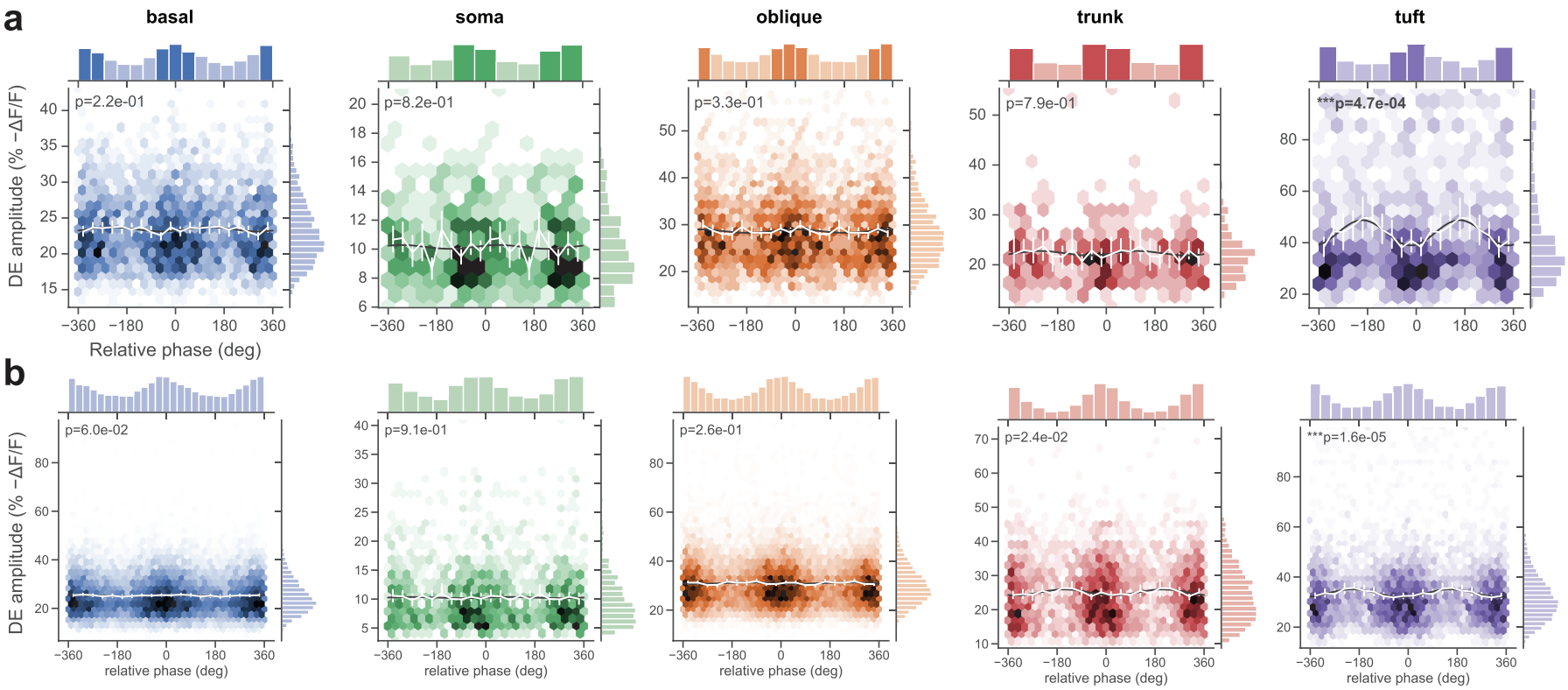

Figure S9. Extended data associated with Fig 2. Theta-phase modulation of DE amplitude across somatic and dendritic regions. 2D histograms of the distribution of DEs in theta phase and amplitude space. Each hexagon corresponds to a single phase/amplitude bin, while color intensity corresponds to the relative density of events within that bin. **a.** DEs from example cell AN092120-1 shown in Fig S8 and **b.** for all cells. Linear-circular fits (black lines; see Methods: Phase modulation of DE amplitude) are shown along with significance level and mean amplitude of DEs per phase bin (white lines) with 95% CI whiskers. Across cells, 2/11 cells showed DE amplitude modulation of at least one region ($\alpha = 0.01$ using the Bonferroni correction).

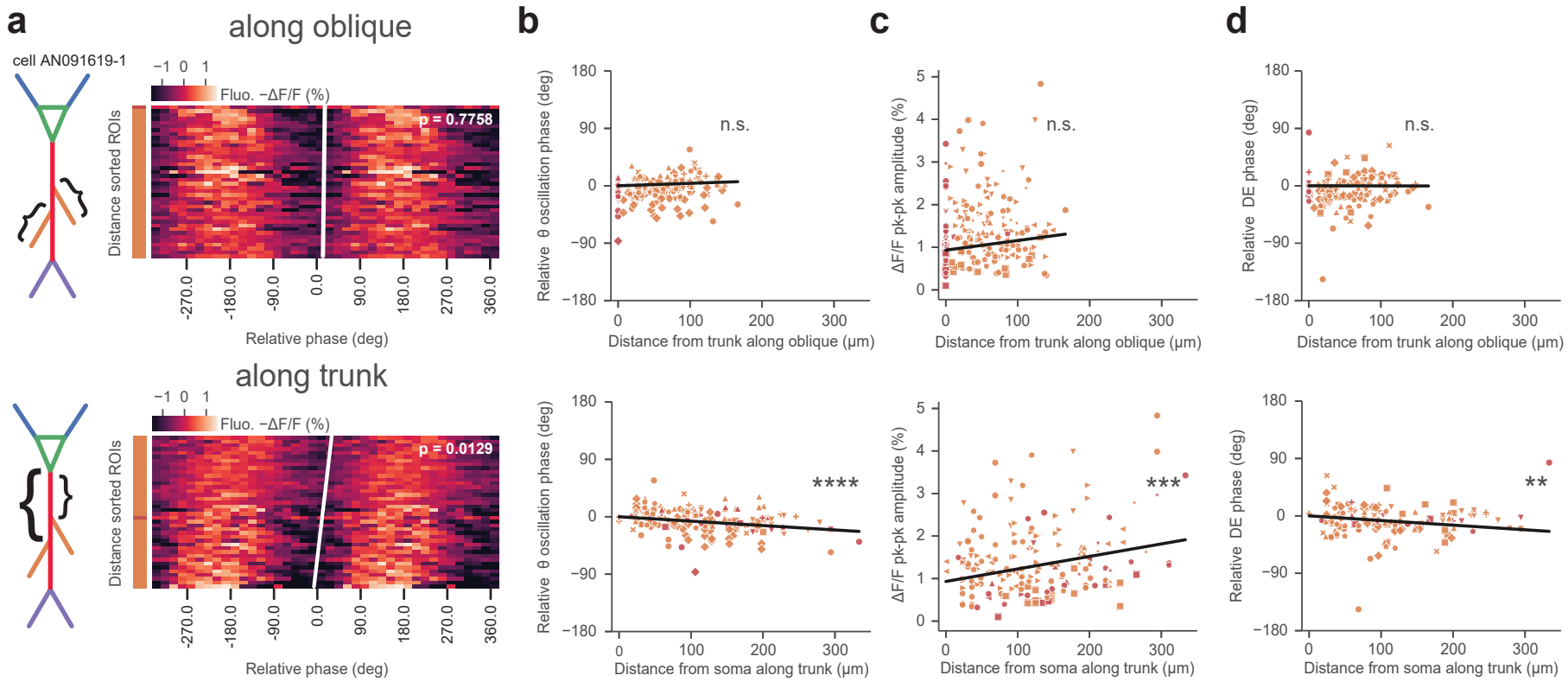

Figure S10. Extended data associated with Fig 2. Theta-band membrane potential oscillation phase, amplitude and DE phase gradients occur along trunk rather than along oblique dendrites. Phase measured relative to the actual or inferred somatic compartment phase. **a.** Theta-band phase-binned $-\Delta F/F$ fluorescence heatmaps of distance-sorted trunk and oblique dendritic ROIs for example cell of Figure 2 along with rank-regression lines, sorted by distance along oblique w.r.t. trunk stem location (top) or along trunk w.r.t. somatic compartment (bottom). Phase advances significantly ($p = 0.0129$) along trunk but not along oblique dendrites ($p = 0.7758$). Multivariate linear regression of theta-band relative fluorescence oscillation phase, $-\Delta F/F$ pk-pk oscillation amplitude and DE phase (**b.** oscillation phase: adjusted $r^2 = 0.18, p < 1.3 \times 10^{-7}$, **c.** oscillation amplitude: adjusted $r^2 = 0.07, p = 0.002$ and **d.** DE phase: adjusted $r^2 = 0.07, p = 0.002$) has a nonsignificant projection against distance along oblique (top row, **b.** oscillation phase: $p = 0.12$, **c.** oscillation amplitude: $p = 0.12$, **d.** DE phase: $p = 0.973$) but significant along trunk (bottom row, **b.** oscillation phase: $p < 1.2 \times 10^{-7}$, **c.** oscillation amplitude: $p = 0.0005$, **d.** DE phase: $p = 0.004$) dendrites for ROIs pooled from all cells.

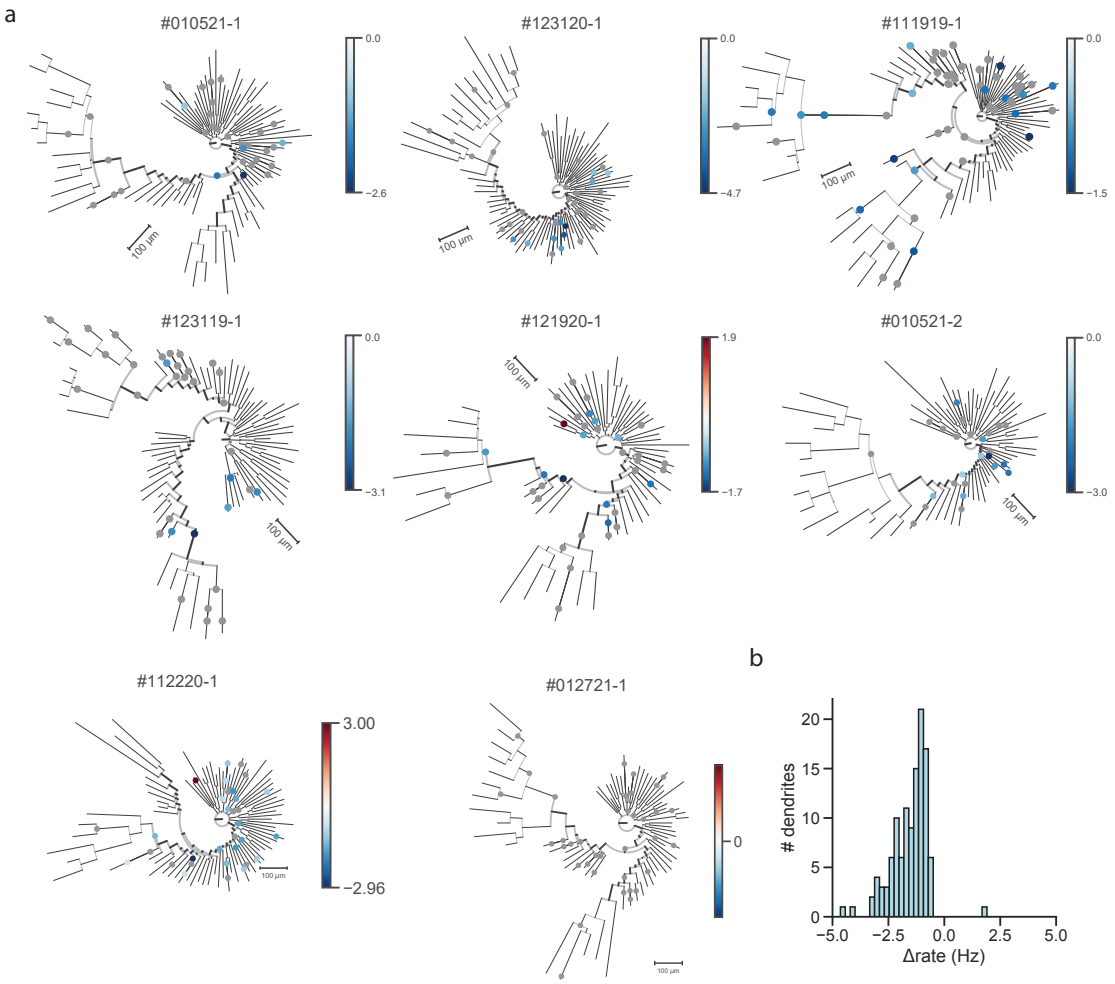

Figure S11. Rate modulation of individual dendrites by SWRs. a. Phylograms of all cells analyzed in Fig 4, with recording locations colored by change in DE rate inside minus outside of SWRs. Grey: Nonsignificantly ripple modulated locations under Poisson rate test. This test is generally conservative given the sparsity of events. 17.7% of dendrites exhibit significant rate modulation around ripples, with the majority suppressing their firing in response to SWRs. **b.** Summary histogram of rate modulation ($r_{inside} - r_{outside}$) at significantly modulated dendrites

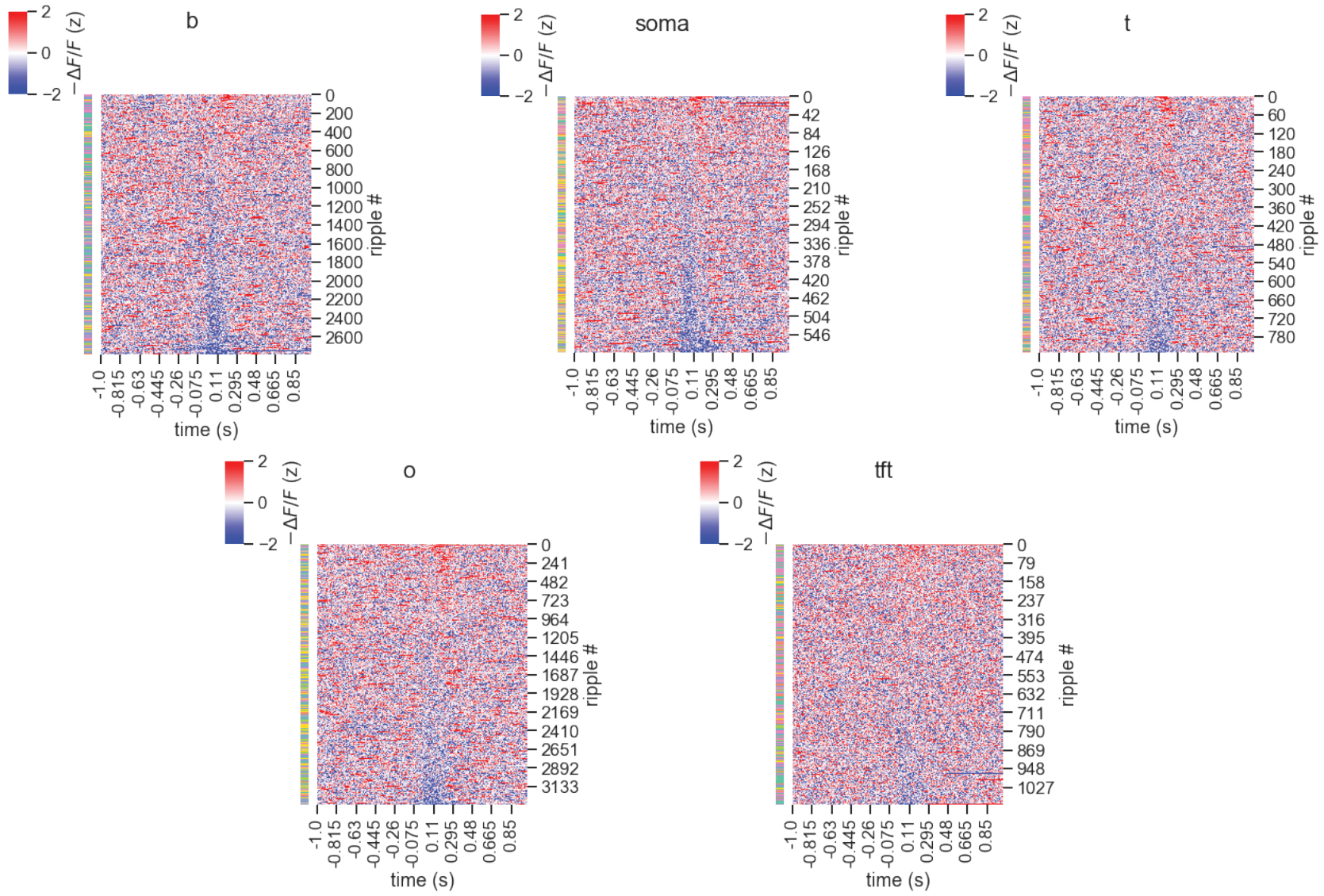

Figure S12. Heatmaps of all ripples shown in Fig 4. Heatmap of z-scored fluorescence around SWRs across all cells and segments by region, sorted by mean activity from 0-250 ms. Row color: cell ID. Inhibition predominates in the peri-ripple zone, but a small proportion of ripples recruit the recorded dendrite.

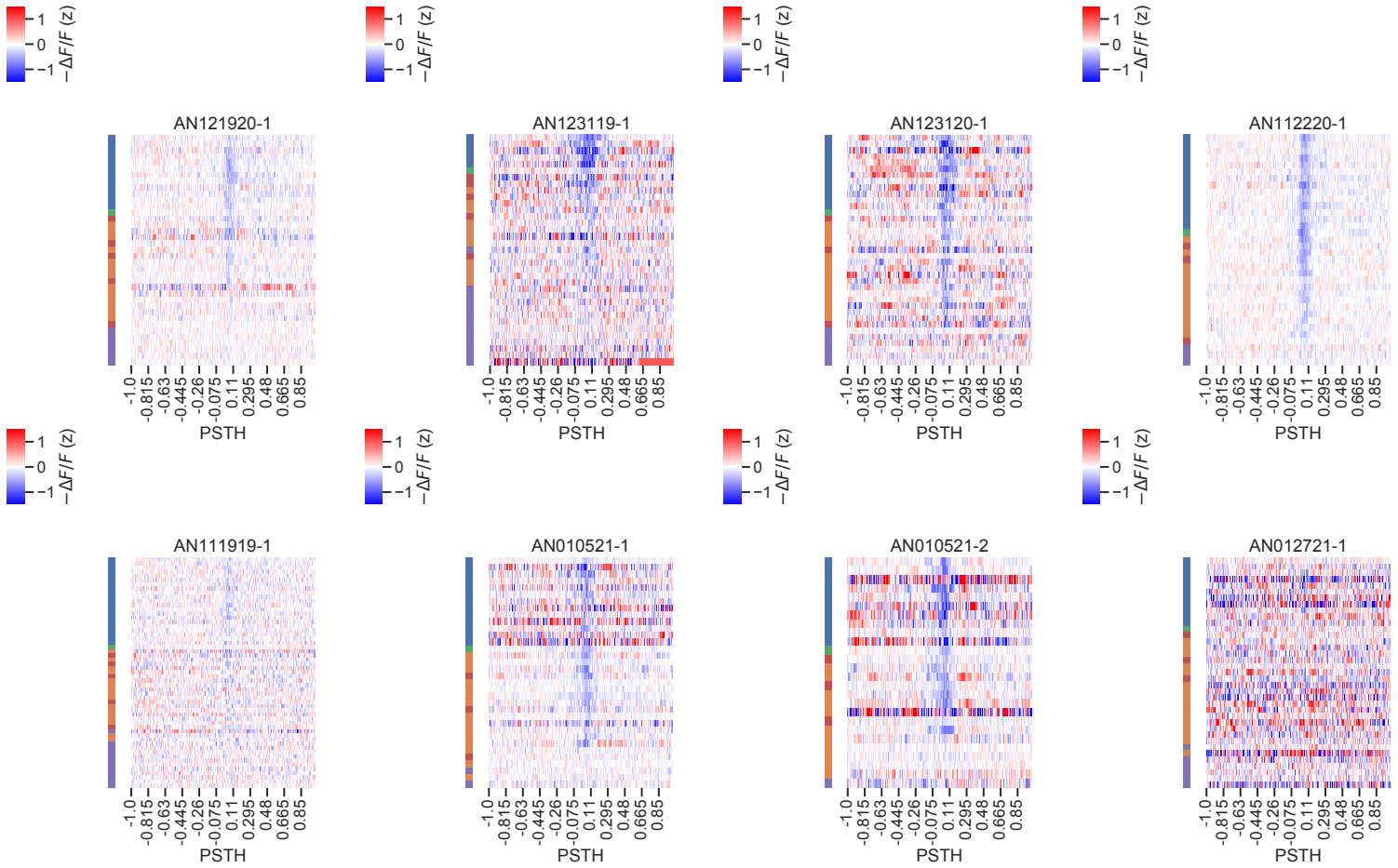

Figure S13. Dendritic hyperpolarization is centered around ripple peak irrespective of soma distance. Similar to our theta analysis of Figure 2, we ask the question of whether anatomical gradients emerge in the dendrite SWR response. Unlike our theta findings, it appears SWR-associated hyperpolarization is centered symmetrically about the ripple peak in all compartments. Mean heatmap of z-scored fluorescence in a ± 1 s window around SWRs (aligned to peak) by cell and segment, sorted by signed soma distance. Row color: recorded region. Inhibition predominates in the peri-ripple zone in most cells and segments. Cell AN012721-1 did not exhibit strong ripple modulation.

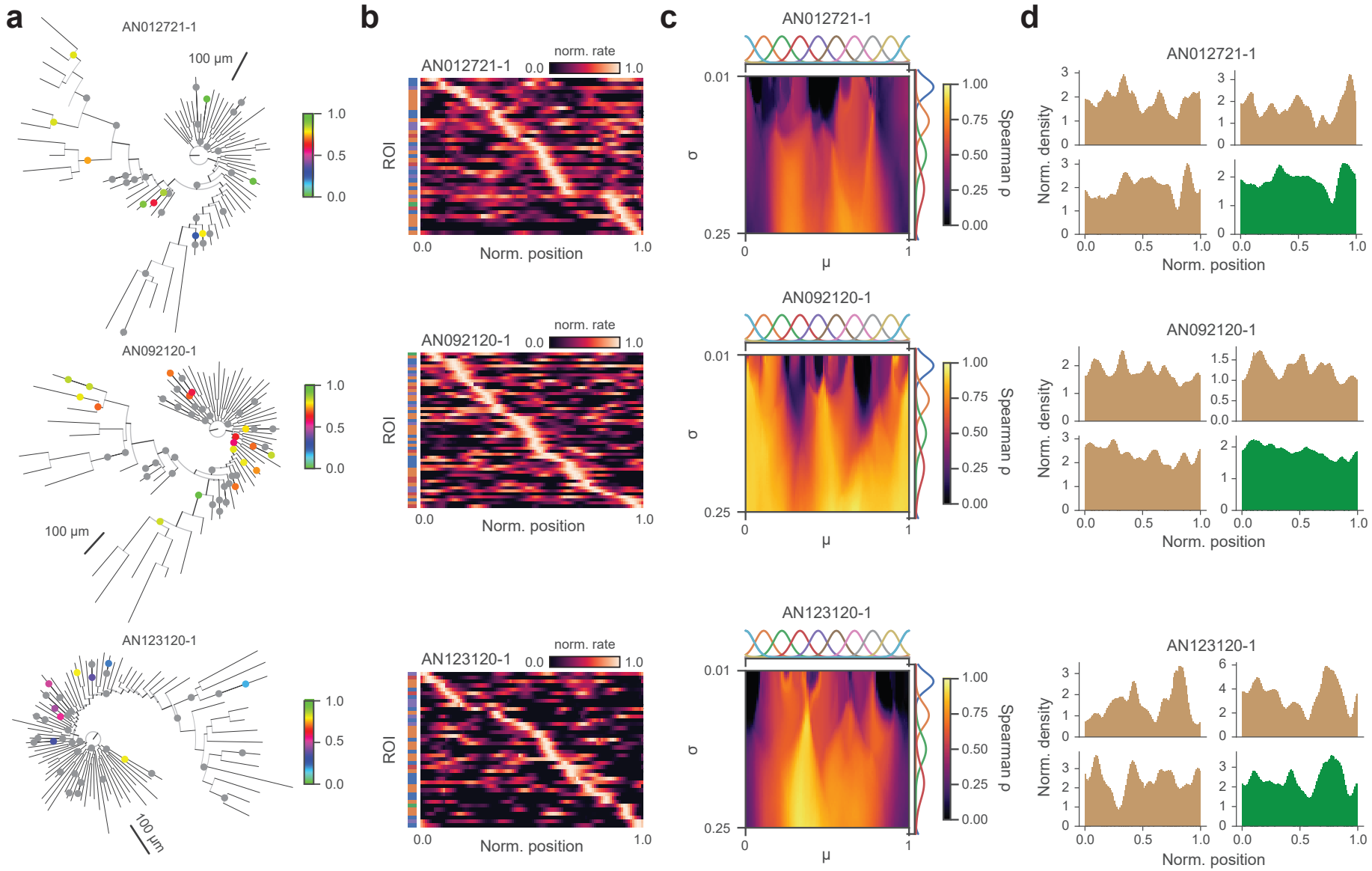

Figure S14. Extended data associated with Fig . We provide further examples of cells from our dataset exhibiting distributed dendritic spatial tuning. Similar to the example we show in the main figure, these cells feature diverse tuning across the dendritic arbor and high expressivity for constructing somatic tuning curves. **a.** Additional example cells, with recording locations colored by tuning centroid. Grey: Nonsignificantly peaked tuning curves under Rayleigh test. **b.** Segment tuning curves associated with cells in **a.**, sorted by tuning curve peak. **c.** Reconstruction fidelity matrix of Fig 5e for example cells shown. **d.** Tuning histograms of primary basal subtrees (brown), with overall basal tuning histogram (green).

Table S1. ASAP3 steady state fluorescence response in HEK293 cells as a function of membrane potential (in mV). Sigmoidal fit coefficients for $F(v) = a + (b - a)/\{1 + \exp[(c - v)/d]\}$.

Temp (°C)	a	b	c	d
22–23	1.93	0.4643	-90.48	38.51
37	2.912	0.4916	-117.5	36.1

Table S2. ASAP3 dynamic step double exponential fit response in HEK293 cells at 37 °C for voltage steps $V_1 \longrightarrow V_2$.

V_1 (mV)	V_2 (mV)	τ_{fast} (ms)	τ_{slow} (ms)	% τ_{fast}
-70	30	0.81	4.32	69
30	-70	3.25	5	58
-70	-100	0.91	4.24	34
-100	-70	1.09	5.84	63
-70	-40	1.02	4.4	50
-40	-70	0.69	4.19	29
-70	0	0.94	4.13	60
0	-70	1.8	5.29	32

region	run modulated	upper	lower	median
basal	0.0	1.40	1.06	1.25
	1.0	0.74	0.63	0.68
oblique	0.0	1.66	1.34	1.55
	1.0	0.87	0.71	0.82
soma	0.0	1.55	0.22	0.88
	1.0	0.74	0.13	0.38
trunk	0.0	1.65	0.86	1.18
	1.0	0.82	0.49	0.70
tuft	0.0	2.11	1.49	1.78
	1.0	1.20	0.98	1.10

Table S3. Data associated with Fig 1f. Median DE frequencies and 95% bootstrapped confidence intervals inside and outside running epochs (all values reported in Hz, $N = 11$ cells)

region	ripple	median	lower	upper
basal	outside	18.9	18.1	19.5
	inside	15.7	13.9	18.3
oblique	outside	20.7	19.9	21.2
	inside	18.9	16.8	21.6
soma	outside	6.7	3.9	8.6
	inside	14.6	n/a	n/a
trunk	outside	16.7	15.4	17.5
	inside	17.0	14.2	19.7
tuft	outside	18.8	16.5	19.5
	inside	17.6	12.9	19.6

Table S4. Data associated with Fig 4d. Median DE peaks and 95% bootstrapped confidence intervals inside and outside SWR epochs (all values reported in $\% - \Delta F/F$)

region	median	lower	upper
basal	40.60	0.0	57.21
oblique	65.27	5.91	77.44
soma	57.50	35.00	87.50
trunk	60.42	15.00	87.83
tuft	6.67	-47.50	71.67

Table S5. Data associated with Fig 4e. Median delay and 95% bootstrapped confidence intervals between LFP SWR power peak vs membrane potential trough (all values reported in ms)

region	ripple	median	lower	upper
basal	inside	0.20	0.05	0.28
	outside	1.04	0.89	1.61
oblique	inside	0.64	0.40	0.88
	outside	1.38	1.14	1.68
soma	inside	0.0	n/a	n/a
	outside	0.55	0.17	1.01
trunk	inside	0.30	0.0	0.58
	outside	1.37	0.82	2.27
tuft	inside	0.72	0.24	1.50
	outside	1.87	1.18	2.19

Table S6. Data associated with Fig 4f. Median DE frequencies and 95% bootstrapped confidence intervals inside and outside SWR epochs (all values reported in Hz)

region	timepoint	median	lower	upper
basal	LFP peak	-1.2	-3.3	-0.5
	fluor trough	-9.5	-15.1	-3.6
oblique	LFP peak	-0.08	-1.6	0.03
	fluor trough	-8.2	-13.3	-4.6
soma	LFP peak	-0.4	-0.8	-0.2
	fluor trough	-1.4	-2.0	-0.7
trunk	LFP peak	-0.4	-1.3	0.1
	fluor trough	-4.8	-7.3	-2.5
tuft	LFP peak	-0.5	-3.6	-0.1
	fluor trough	-12.4	-16.3	-6.2

Table S7. Data associated with Fig 4h. Median membrane potential and 95% bootstrapped confidence intervals at LFP SWR power peak vs membrane potential trough (all values reported in $\% - \Delta F/F$)

region	condition	upper	lower	median
basal	nonripple	31.92	20.73	25.00
	ripple	42.04	10.17	27.31
oblique	nonripple	30.06	19.98	25.98
	ripple	21.67	12.62	16.06
trunk	nonripple	33.25	16.38	28.00
	ripple	35.18	3.04	17.03
tuft	nonripple	19.61	15.12	16.14
	ripple	21.08	12.75	18.00

Table S8. Data associated with Fig 4i. Median DE FWHM and 95% bootstrapped confidence intervals inside and outside SWR epochs (all values reported in ms